

# Coiling and Supercoiling of Vortex Filaments in Oscillatory Media

Guillaume Rousseau<sup>1,2</sup>, Hugues Chaté<sup>1</sup>, and Raymond Kapral<sup>3</sup>

<sup>1</sup>*CEA — Service de Physique de l'Etat Condensé, Centre d'Etudes de Saclay, 91191 Gif-sur-Yvette, France*

<sup>2</sup>*DAEC — Observatoire de Meudon, 5, place Jules Janssen, 92195 Meudon, France*

<sup>3</sup>*Chemical Physics Theory Group, Department of Chemistry, University of Toronto, Toronto, ON M5S 3H6, Canada*

We study the behavior of vortex filaments subject to a uniform density of phase twist in oscillatory media described by the complex Ginzburg-Landau equation. The first instability is a supercritical Hopf bifurcation to stable propagating helical vortices. The secondary instability, also a forward Hopf bifurcation, leads to quasiperiodic supercoiled filaments. The structural changes undergone by these dynamical objects are akin to those of twisted elastic rods, in spite of the presence of the ribbon component of the twist, particular to phase singularities.

Spontaneous oscillations in nonlinear extended media are commonly observed in nature. Examples include reaction-diffusion systems [1], certain regimes of fluid flows [2], and biological systems with intrinsic clocks [3]. The complex Ginzburg-Landau equation (CGLE) [2,4]:

$$\partial_t A = A + (1 + i\alpha)\nabla^2 A - (1 + i\beta)|A|^2 A, \quad (1)$$

where  $A$  is a complex amplitude describing the slow modulations of the oscillations and  $\alpha$  and  $\beta$  are two real parameters, plays a central role in the analysis of the behavior of oscillatory media, especially since its validity extends far beyond the vicinity of the Hopf bifurcation where it can be formally derived. [5]

The CGLE exhibits the localized structures that often determine the spatiotemporal organisation of the medium. In two dimensions,  $A = 0$  generically at point vortices which may be sources of spiral waves. In three space dimensions, the topological defects are filaments around which “scroll waves” can be emitted. The defects are phase singularities, determined by the topology of the phase field  $\arg A$ . Consequently, they are not described solely by their geometrical structure as given by the Frenet frame at each point along the filament; one must also specify how the phase field itself is twisted along the vortex (ribbon twist). [6]

As in lower space dimensions, the structure and dynamics of three-dimensional (3D) phase singularities is best studied in the parameter region where the scroll waves are stable. Recent simulations and analytical studies in this region [7] have shown that initially prepared untwisted vortex rings shrink and disappear. Disordered states [8] and helical structures [9] arising from spontaneous stretching and bending of untwisted vortex filaments have been found in this region.

In this Letter, we investigate numerically the effects of a finite uniform density  $\gamma$  of ribbon twist per unit length on the simplest configuration, a straight infinite filament in the regime where both the emitted scroll waves and the 2D spiral cores are stable. While the limit of small twist was discussed in [7], a detailed study of the effects of twist has not been carried out for the CGLE, even

though twisted filaments are easily found in the chaotic regimes of the 3D CGLE [10] and have also been observed in experiments on the Belousov-Zhabotinsky (BZ) reaction in the excitable regime. [11] We find that there is a finite twist density  $\gamma_c(\alpha, \beta)$  beyond which the infinite filament undergoes a supercritical Hopf bifurcation which saturates to produce helical vortices. We also characterize the secondary instability, which takes the form of another Hopf bifurcation leading to the supercoiling of the primary helices. These two bifurcations are analyzed from a topological viewpoint. In particular, the writhe is a linear function of the excess twist after the first instability, and the ribbon twist also varies linearly. This suggests analogies between the dynamical structures observed and the behavior of twisted elastic rods.

Our results extend similar early observations in excitable media. [12] Of special relevance to the present work are studies of helical solutions of various reaction-diffusion models [12–14] which have shown that an initially straight vortex filament may adopt a helical form with fixed radius for large enough twist. Helical filaments have also been observed in 3D magnetic resonance images of the BZ reaction. [15] We believe our findings apply to the excitable case and put those results in a more general setting by elucidating the dynamical nature of the instabilities. Our work should also lead to an understanding of the behavior of more general twisted vortex lines.

The spiral solution of the 2D CGLE is important for the study of 3D vortex lines: cross sections of scroll waves are spirals, up to correction terms calculated in [7]. The spiral solution is given in polar coordinates  $(r, \theta)$  by

$$A_s(r, \theta, t) = F(r) \exp i[\omega_s t \pm \theta + \psi(r)], \quad (2)$$

with  $\omega_s = -\beta + k_s^2(\beta - \alpha)$ , where  $F(r)$  and  $\psi(r)$  are two real functions whose asymptotic behavior for  $r \rightarrow 0$  and  $r \rightarrow \infty$  is known, and  $k_s$  is the asymptotic wave number. [16] In spite of the absence of a general explicit form, many properties of this solution are known, in particular in the parameter region where the asymptotic emitted planewave and the discrete core modes are linearly stable. [17] We first consider straight twisted filaments in this domain of the  $(\alpha, \beta)$  plane and use the 2D stable

spiral solution to generate initial conditions efficiently by shifting the phase of the spiral regularly along the third spatial dimension  $z$  to create twist:  $\theta \rightarrow \theta + \gamma z$ . In the numerical simulations reported below, such initial conditions have been used in finite boxes of “height”  $L_z$  with periodic boundary conditions in  $z$ , so that the total twist is a multiple of  $2\pi$ :  $\gamma L_z = 2\pi n_t$ .

The link number  $Lk$ , total twist  $Tw$  and writhe  $Wr$  of the filament ribbon obey the following law [18,6]:

$$Lk = Tw + Wr = Tw_f + Tw_r + Wr \quad , \quad (3)$$

where  $Tw_f = \oint \tau(s) ds$  and  $Tw_r = \oint (d\varphi/ds) ds$  are, respectively, the total Frenet and ribbon components of the twist, defined here in terms of local quantities calculated in the Frenet frame  $(\mathbf{t}, \mathbf{n}, \mathbf{b})$  parametrized by the arclength  $s$ , the torsion  $\tau$  and the angle  $\varphi$  between a given ribbon curve and the binormal vector  $\mathbf{b}$ . For closed 3D ribbons, the link number  $Lk$  is invariant [6]. In finite boxes periodic in  $z$ , it is conserved if the ribbon is not “cut”, i.e. no reconnection occurs, either of the filament with itself or with another filament, and we have, simply:

$$Lk = 2\pi n_t = \gamma L_z \quad . \quad (4)$$

The constraint imposed by the conservation law has important consequences since it implies that filaments with different  $\gamma$  values are not continuously related; thus, one must consider  $\gamma$  as an independent parameter.

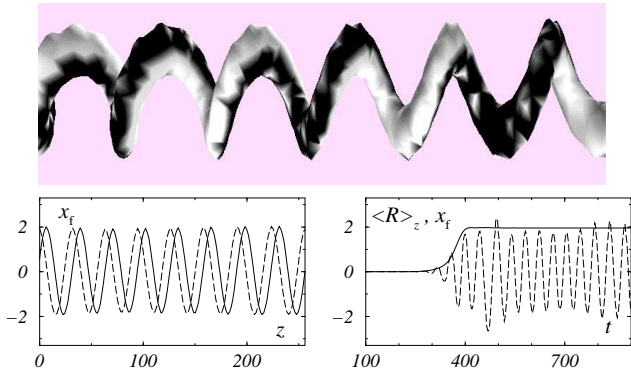


FIG. 1. Stable helical vortex for  $\alpha = 1.7$ ,  $\beta = 0$ ,  $\gamma = 0.098$  and  $L_z = 512$  ( $L_x = L_y = 128$ ). Top: perspective view of the 3D isosurface  $|A| = 0.6$  colored by the phase field ( $2\pi$ -periodic grey scale). Note the presence of ribbon twist ( $\gamma_h = 0.196$ ,  $Tw_r/L_z = -\gamma$ ). Bottom left:  $(x, z)$  projection of the filament at  $t = 2495$  (dashed line) and  $t = 2500$  (solid line). Bottom right: growth of  $\langle R \rangle_z$  (solid line) and time series of the  $x$  coordinate (dashed line) of a point on the filament at a given  $z$ .

Consider a single twisted filament, generated as described above, evolving under the CGLE. Our simulations employed no-flux boundary conditions in the  $x$  and  $y$  directions while the box was periodic in  $z$ , the axis of the filament. All numerical results have been checked by changing the box size and the spatiotemporal mesh size.

For small  $\gamma$ , the solution quickly relaxes to take into account the wavenumber and frequency shifts [7] between

the 2D spiral waves and the 3D scroll waves. This (stable) solution of the 3D CGLE is  $A_f(r, \theta, z, t)$ :

$$A_f = \sqrt{1 - \gamma^2} F(r') \exp i[\omega_f t \pm (\theta + \gamma z) + \psi(r')] \quad , \quad (5)$$

where  $r' = r\sqrt{1 - \gamma^2}$  and  $\omega_f = \omega_s(1 - \gamma^2) - \gamma^2\alpha$ , with  $\omega_s$ ,  $F$ , and  $\psi$  given by the 2D spiral solution (2). We have confirmed that our numerical solutions coincide with the above exact solution when there is no core instability.

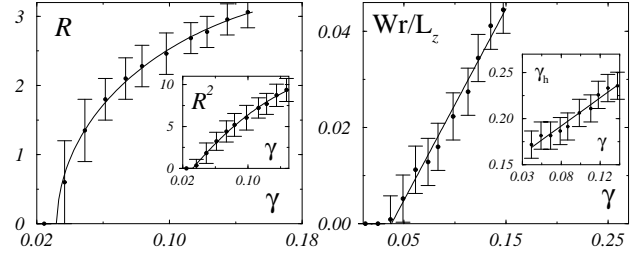


FIG. 2.  $\alpha = 1.7$  and  $\beta = 0$ :  $R(\gamma)$  (left) and  $Wr(\gamma)/L_z$  (right) ( $\gamma_c \simeq 0.032$ ). Insets:  $R^2(\gamma)$  (left) and  $\gamma_h(\gamma)$  (right).

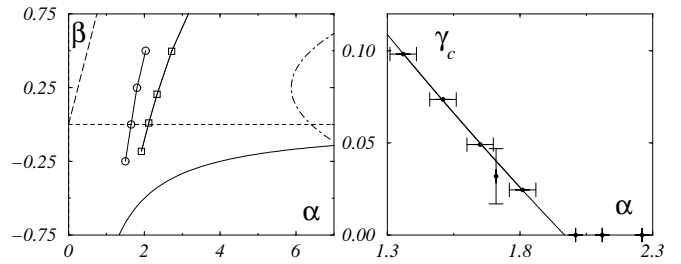


FIG. 3. Left: phase diagram of the 3D CGLE. The region of interest lies between the 2D spiral core instability (dash-dotted) line, the phase instability  $1 + \alpha\beta = 0$  (solid line), and the  $\alpha = \beta$  line (dashed) where the spiral core is infinite. The thin lines are the  $\gamma_c = 0.049$  (circles) and  $\gamma_c = 0$  (squares, from [9]) level curves of the  $\gamma_c(\alpha, \beta)$  surface. Right:  $\gamma_c(\alpha)$  for  $\beta = 0$ . A quadratic fit gives  $\gamma_c = 0$  for  $\alpha = 1.95(15)$ .

For large enough  $\gamma$  this relaxation is followed by the growth of periodic modulations along the filament, which becomes a helix of pitch  $\lambda_h$  and well-defined radius  $R$  (Fig. 1). The helix rotates with constant angular velocity  $\omega$  and any point on the helix moves along its axis at a constant velocity  $v = \omega/\gamma_h$  with  $\gamma_h \equiv 2\pi/\lambda_h$ . These results indicate that the straight filament has undergone a Hopf bifurcation to traveling waves. The direction of propagation and rotation is determined by the sign of  $\gamma$ , which breaks the  $z \rightarrow -z$  parity symmetry. Varying  $\gamma$  continuously across the instability threshold  $\gamma_c$ , the behavior expected for a supercritical bifurcation is observed:  $R^2 \sim (\gamma - \gamma_c)$ , while  $v$  and  $\lambda_h$  vary smoothly (Fig. 2). The forward nature of the bifurcation is confirmed by the growth transient (Fig. 1 bottom right). Similarly, keeping  $\gamma$  constant and varying  $(\alpha, \beta)$  toward the 2D core-instability line, a bifurcation point is passed and the expected small- $R$  behavior (e.g.  $R^2 \sim (\alpha - \alpha_c)$  at

fixed  $\beta$ ) is observed (not shown). This suggests the existence of a critical surface  $\gamma_c(\alpha, \beta)$  delimiting the stability of straight twisted filaments. Our simulations yielded the approximate location of the  $\gamma_c = 0.049$  line in the  $(\alpha, \beta)$  plane (Fig. 3 left). The complete  $\gamma_c(\alpha, \beta)$  surface could be determined from a linear stability analysis of solution (5), possibly along the lines of [9], a rather difficult task left for future work [10].

The  $\gamma_c = 0$  line determines the stability domain of the untwisted filament. In [8], it was argued that this solution, which is just the trivial extension of the 2D spiral, is unstable in the region of the 2D core instability. It was further argued recently that the instability region of the untwisted filament extends beyond the 2D core line [9]. To attack this problem from the viewpoint of twisted filaments, we have performed simulations for  $\beta = 0$  to determine  $\gamma_c(\alpha)$  (Fig. 3 right). We find, by extrapolation,  $\gamma_c = 0$  for  $\alpha = 1.95(15)$ , in agreement with [9]. Our results indicate that the instability of the  $\gamma = 0$  filaments does *not* lead to helices. In this special case, the  $z \rightarrow -z$  parity symmetry is preserved and one expects, a priori, the superposition of opposite traveling waves at the linear stage. At the nonlinear level, we observe the saturation of the two corresponding amplitudes at the same value and the appearance of a flat,  $z$ -periodic filament rotating uniformly around the  $z$  axis, the equivalent of standing waves in the amplitude representation (Fig. 4).

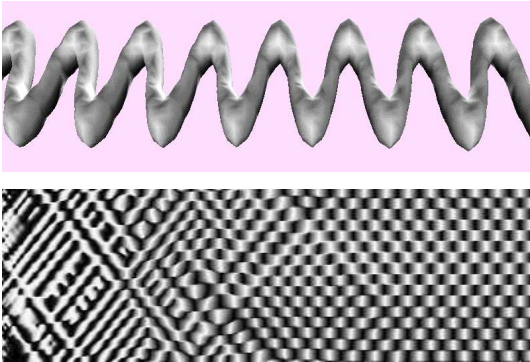


FIG. 4. Asymptotic state of an unstable untwisted filament ( $\alpha=2.5$ ,  $\beta=0$ ). Top: 3D isosurface  $|A| = 0.6$  colored by the phase field. Bottom: space-time plot ( $t$  running from left to right) of the phase  $\phi(z, t) = \arctan(y_f(z)/x_f(z))$  where  $(x_f(z), y_f(z), z)$  parametrize the filament. ( $2\pi$ -periodic grey scales 0=black,  $\pi$ =white, were used).

We now consider our results at non-zero twist from a topological viewpoint. Since no reconnection occurs across the transition,  $Lk$  remains constant. Given  $\lambda_h$  and  $R$ , all terms of conservation law (3) can be calculated easily. For the straight filament, the Frenet frame is degenerate;  $Tw_f$  and  $Tw_r$  cannot be distinguished. For the stable helix, on the other hand, the ribbon twist is given by  $Tw_r/Lk = 1 - \gamma_h/\gamma$ . Moreover,  $\kappa$  and  $\tau$  are constant along the  $z$  axis:  $\kappa/(R\gamma_h) = \tau = \gamma_h/(1 + R^2\gamma_h^2)$ . We then have [13]:

$$\frac{Tw_f}{Lk} = \frac{\gamma_h}{\gamma} - \frac{Wr}{Lk} = \frac{\gamma_h}{\gamma\sqrt{1 + R^2\gamma_h^2}}. \quad (6)$$

Exploring a large part of the  $(\alpha, \beta)$  domain of interest, we consistently found that  $\lambda_h$  is larger than  $\lambda_s$ , the wavelength of the 2D spiral, but of the same order, and that the two wavelengths vary similarly with  $(\alpha, \beta)$  [10]. Thus the typical scale of the 3D instability depends essentially on the wavenumber selected by 2D spiral solution. We also find that  $\gamma_h > \gamma$ , which implies that  $Tw_r < 0$ . The ribbon twist “compensates” the strong torsion due to the instability. For  $(\alpha = 1.7, \beta = 0)$ ,  $\lambda_h$  decreases with increasing  $\gamma > \gamma_c$  (Fig. 2, right), and thus the magnitude of the  $Tw_r$  increases. In fact, our data indicates a linear variation with  $\gamma$ , but we cannot rule out a weakly quadratic dependence. Moreover, in agreement with (6) for small  $R^2 \sim \gamma - \gamma_c$ ,  $Wr \sim (\gamma - \gamma_c)$ , but, remarkably, this behavior also extends far from  $\gamma_c$  (Fig. 2). (Again, a weakly quadratic dependence is still possible.) Thus, all topological quantities seem to vary linearly above threshold, and, in particular, a *constant proportion* of the excess twist  $\gamma - \gamma_c$  is converted into writhe. This is akin to the behavior of elastic rods [6,20].

Moving away from the  $\gamma_c(\alpha, \beta)$  surface, the filament undergoes a secondary instability at some critical value  $\gamma'_c > \gamma_c$ : a long-wavelength modulation appears on the stable regular helix, eventually producing a supercoiled filament (Fig. 5). No reconnection event is observed. This structure is characterized by two well-defined wavelengths,  $\lambda_1$  and  $\lambda_2$ , with  $\lambda_1 \sim \lambda_h$  and  $\lambda_2 \gg \lambda_h$  (Fig. 5, middle left). In general, for an infinite filament, the two wavelengths are incommensurate and the superhelix is a quasiperiodic object whose projection on the  $(x, y)$  plane produces a characteristic “flower” pattern (middle right). Associated with these wavelengths are two frequencies, or two velocities  $v_1$  and  $v_2$  (middle left).

The secondary instability is also a supercritical Hopf bifurcation. Its forward nature and the nonlinear saturation are apparent in the time evolution of an initially straight filament, which quickly turns into a weakly unstable helix before bifurcating toward a superhelix (Fig. 5, bottom left). Varying  $\gamma$ , the mean radius  $\langle R \rangle_z$  is continuous but not differentiable at  $\gamma'_c$ , and the amplitude of the secondary modulations can be measured by  $\langle R \rangle_z - R_h$ , where  $R_h$  is the radius of the (unstable) primary helix (measured, e.g., from the transient helix stage) (Fig. 5 bottom right). As expected for a forward Hopf bifurcation, near threshold our data is consistent with  $(\langle R \rangle_z - R_h)^2 \sim (\gamma - \gamma'_c)$ . Even though the amplitude of this secondary instability saturates, we cannot rule out a chaotic asymptotic behavior.

Our measurements (from Fourier spectra) show that  $1/\lambda_h = 1/\lambda_1 + 1/\lambda_2$ , at least for  $\gamma - \gamma'_c$  not too large. Since the link number  $Lk$  is constant (no reconnection occurred), this relation implies that the ribbon component of the twist  $Tw_r$  varies smoothly across the transition. [6] This is corroborated by direct measurements of  $Tw_r$  and the other topological quantities ( $Wr$ ,  $Tw_f$ )

across the secondary instability. During the evolution shown in Fig. 5 (bottom left),  $Wr(t)$  is constant through the second morphological change (bottom left) since the mean torsion remains constant;  $\tau(s)$ , however, becomes  $\lambda_1$ -periodic. Finally, the available data does not allow to decide whether these quantities still vary linearly with  $\gamma$ .

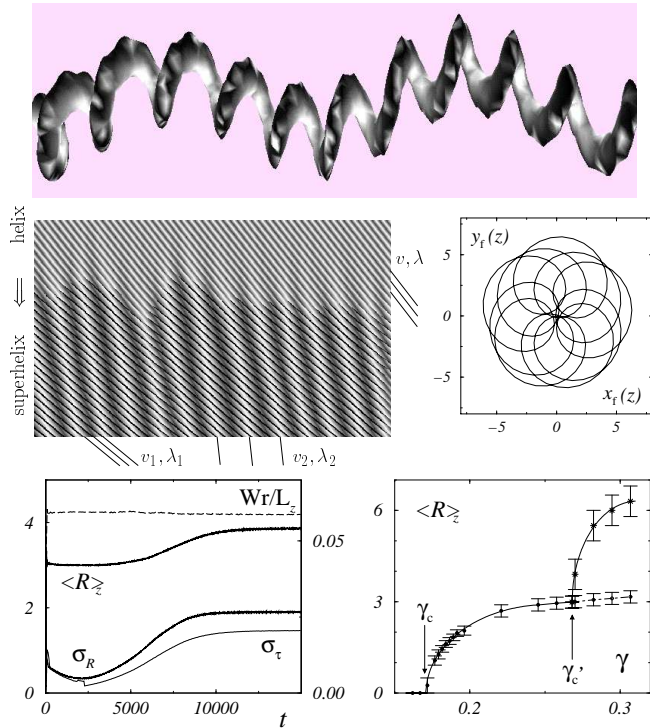


FIG. 5. Secondary Hopf bifurcation for  $\alpha = 1$  and  $\beta = -0.5$ . This data was obtained under the constraint that  $Tw_r = 0$ , a small perturbation here, since  $\gamma_h \simeq \gamma$  for these parameter values. Top:  $\gamma = 0.27$ ; 3D isosurface  $|A| = 0.6$  colored by the phase field ( $2\pi$ -periodic grey scale); Middle left: space-time plot of  $\phi(z, t)$  (see Fig. 4). Portion of size  $L = 600$  of a box of length  $L_z = 2048$  shown during  $\Delta t = 1825$  with an initial straight filament ( $L_x = L_y = 92$ ,  $\gamma = 0.295$ ).  $2\pi$ -periodic grey scale (0 = black,  $\pi$  = white), except for the points where  $\partial_z \phi < 0$  which are plotted in black regardless of the value of  $\phi$ . This enhances the “petals”, or small loops, in the superhelix, since only points of these loops have negative  $\partial_z \phi$ . For the primary helix, observed as a transient,  $\partial_z \phi = \gamma_h > 0$  everywhere. Wavelengths  $\lambda_h$ ,  $\lambda_1$ , and  $\lambda_2$  and velocities  $v$ ,  $v_1$  and  $v_2$  are indicated. Middle right: projection of superhelix on the  $(x, y)$  plane. The flower pattern is periodic due to the finite box length. Bottom left:  $\gamma = 0.27$ : time series of  $\langle R \rangle_z$  and  $\sigma_R$  its rms over  $z$  (left scale),  $Wr/L_z$  and  $\sigma_\tau$  the rms of the torsion (right scale). Bottom right:  $\langle R \rangle_z(\gamma)$  across the two bifurcation points  $\gamma_c \simeq 0.171$  and  $\gamma'_c \simeq 0.267$ . Dashed line:  $R_h$  for the (weakly) unstable helices.

Although the instabilities studied here are rather traditional Hopf bifurcations, they are topologically constrained. The existence of the ribbon component of the twist, particular to the filaments studied here, comes into play in a somewhat “passive” way. Associated to the soft

phase mode, it can be seen as accommodating the torsion and writhe of the bifurcated structure. Indeed, although it is a dynamical object supporting propagating waves, our filament coils and supercoils under twist like an elastic rod or a DNA molecule (see [6,20] and references therein). Moreover, the simple behavior of  $Wr$  supports the adoption a topological viewpoint when studying the dynamics of 3D phase singularities. We note, however, that the ribbon twist might play a more important role in excitable media or systems with complex oscillations, for which the gauge invariance of the phase is lost.

- 
- [1] *Chemical Waves and Patterns*, eds. R. Kapral and K. Showalter, (Kluwer, Dordrecht, 1994).
  - [2] M. C. Cross and P. C. Hohenberg, *Rev. Mod. Phys.* **65**, 851 (1993).
  - [3] A. Goldbeter, *Biochemical Oscillations and Cellular Rhythms*, (Cambridge U. P., Cambridge, 1996); A. T. Winfree, *When Time Breaks Down*, (Princeton U. P., Princeton, NJ, 1987).
  - [4] Y. Kuramoto, *Chemical Oscillations, Waves and Turbulence*, (Springer, Berlin, 1984); A. C. Newell, *Envelope Equations*, (Am. Math. Soc., Providence, RI, 1974).
  - [5] For recent experimental examples, see, e.g., T. Leweke and M. Provansal, *Phys. Rev. Lett.* **72**, 3174 (1994); Q. Ouyang and J.-M. Flesselles, *Nature* **379**, 6561 (1996).
  - [6] M. Tabor and I. Klapper, *Nonlin. Sc. Today*, **4:1**, 7 (1994); **4:2**, 12 (1994).
  - [7] M. Gabbay, E. Ott and P. N. Guzdar, *Phys. Rev. Lett.* **78**, 2012 (1997).
  - [8] I. S. Aranson and A. R. Bishop, *Phys. Rev. Lett.* **79**, 4174 (1997).
  - [9] I. S. Aranson, A. R. Bishop and L. Kramer, xxx.lanl.gov e-Print archive, patt-sol/9712004.
  - [10] G. Rousseau, H. Chaté, and R. Kapral, in preparation.
  - [11] A. M. Pertsov, R. R. Aliev and V. I. Krinsky, *Nature* **345**, 419 (1990).
  - [12] For a review see, A. T. Winfree, *SIAM Rev.* **32**, 1 (1990); in [1], p. 1.
  - [13] C. Henze, E. Lugosi and A. T. Winfree, *Can. J. Phys.* **68**, 683 (1990).
  - [14] J. P. Keener, *Physica D* **269** (1988); J. J. Tyson and J. P. Keener, in [1], p. 93.
  - [15] A. Cross, *The Development of 3D MRI of the BZ Reaction*, Ph.D. thesis, U. of New Brunswick, 1998.
  - [16] P.S. Hagan, *SIAM J. Appl. Math.* **42**, 762 (1982).
  - [17] I.S. Aranson, L. Kramer, and A. Weber, *Phys. Rev. Lett.* **72**, 2316 (1994).
  - [18] J. H. White, *Am. J. Math.* **91**, 693 (1969).
  - [19] With no-flux conditions in  $z$ , the link would not be a conserved quantity, complicating further the picture.
  - [20] A. Goriely and M. Tabor, *Phys. Rev. Lett.* **77**, 3537 (1996); *Physica D* **105**, 20 (1997); *ibid.* **105**, 45 (1997); preprint (1997), to appear in *Proc. Roy. Soc. A*.